

# Corrosion Prevention of Copper in 2.0 M Sulfamic Acid Using Novel Plant Extract: Chemical, Electrochemical, and Theoretical Studies

Aya. M. Salem\* and Merfat S. Al-Sharif\*

Cite This: *ACS Omega* 2023, 8, 49432–49443

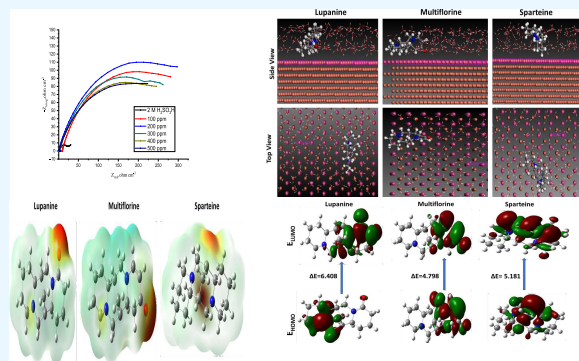
Read Online

ACCESS |

Metrics &amp; More

Article Recommendations

**ABSTRACT:** Copper corrosion was suppressed when a lupine extract was immersed in a 2 M sulfamic acid ( $\text{H}_2\text{NSO}_3\text{H}$ ) solution. Numerous methods, including mass loss (ML), dynamic potential polarization (PL), and electrochemical impedance (EIS), were employed in these experiments, in addition to theoretical computations such as density functional theory (DFT), Fukui function, and Monte Carlo simulations. Fourier transform infrared (FT-IR) spectroscopy and scanning electron microscopy (SEM) were used to analyze the Cu surface's composition and determine its form. Mass loss (ML) was used to examine the inhibition rate of copper corrosion in sulfamic acid at 25 °C in the presence of lupine extract. After examining how it behaved throughout the adsorption process on copper, it was discovered that it follows the Langmuir isotherm and chemical adsorption. An analysis of the PL curves indicates that the lupine extract is a mixed-type inhibitor. It was shown that the inhibitory efficiency increased to 84.2% with increasing lupine concentration. Additionally, as the data show, the efficiency of inhibitors is diminished by increasing temperatures. Theoretical calculations and experimental data were compared using Monte Carlo simulation (MC) and density functional theory (DFT).

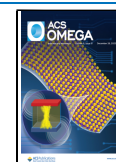


## 1. INTRODUCTION

Sulfamic acid ( $\text{H}_2\text{NSO}_3\text{H}$ ) is used in a variety of industrial operations, such as mechanical cleaning and deposit removal.<sup>1</sup> Unlike chloride, sulfuric acid does not create pitting or fatigue cracking when applied to copper. Instead of producing corrosive fumes, the  $-\text{NH}_2$  and  $-\text{OH}$  functional groups in water solutions of sulfamic acid dissolve the incrustations so they can be removed. A corrosion inhibitor must be present in the sulfamic acid solution to stop corrosion from harming metal surfaces.<sup>2</sup> The earliest metal that humans found and used is copper, which is widely used in a variety of industries, including manufacturing, national defense, light, electrical, and machinery. To prevent copper from being destroyed and to guarantee that copper equipment functions well for the duration of its life, significant measures must be taken. Under certain conditions, copper is susceptible to harmful corrosion, particularly in aggressive corrosive environments like industrial and marine settings.<sup>3–7</sup> Because synthetic organic corrosion inhibitors are bad for the environment, researchers are striving to create green corrosion inhibitors that are nontoxic.<sup>8,9</sup> They function by organic inhibitors adhering to a substrate made of metal. While electrons are given away in lone pairs during electrostatic adsorption, they are given away in pairs with opposing charges during chemical adsorption. We can better comprehend the adsorption mechanism by delineating distinct thermodynamic and kinetic characteristics. Inorganic chemicals such as chromates, nitrites,

dichromate, etc. as well as organic compounds with pi bonds and heteroatoms that boost the compound's effectiveness make up the majority of corrosion inhibitors and play a significant part in preventing corrosion. Due to their N, O, and S composition, organic compounds are good corrosion inhibitors, but their toxicity prevents their use on a large scale. The current research aims to develop a low-cost, environmentally safe, and high-inhibition-efficiency, as well as eco-friendly corrosion inhibitor. Plant extracts can be used to create corrosion inhibitors because of their availability, harmless characteristics, and harmless characteristics. Depending on how they are removed, plant parts can be converted to corrosion inhibitors in a variety of ways. Green corrosion inhibitors can be made from a variety of plant parts including fruits, seeds, flowers, and leaves. The food industry considers lupins, which are underutilized legumes, of particular interest due to their high protein and fiber contents and low starch content. Unlike most other legumes, lupine has oil in it. Although lupins have demonstrated their nutritional and

**Received:** October 19, 2023  
**Revised:** November 24, 2023  
**Accepted:** November 30, 2023  
**Published:** December 14, 2023



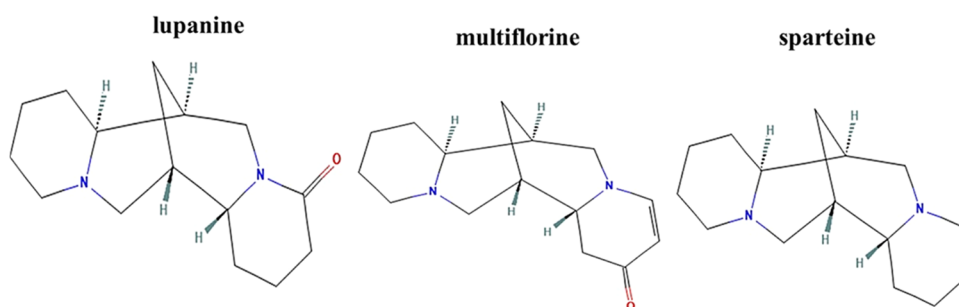


**Figure 1.** Chemical composition of main components in lupine extract.

functional advantages, their main application is in animal feed, and they are not yet widely utilized in human nutrition.<sup>10,11</sup> Up to 50% of quinolizidine alkaloids, 20% of lipids, and 5% of protein can be found in the lupine (*Lupinus* sp. L.) seed content. A genus of plants in the legume family *Fabaceae*, *Lupinus*, is often known as lupine, lupine, or regionally as bluebonnet, among other names. Over 199 species make up the genus, with North and South America serving as its diversity hotspots. The Mediterranean and North Africa both have smaller centers.<sup>12,13</sup> Although they are widely planted for both food and decorative purposes, they are invasive in some locations. In order to prevent corrosion, researchers are concentrating on creating low-cost, nontoxic, biodegradable, and environmentally friendly natural products of plant origin. Inhibitors made from plant extracts are increasingly being used to slow down corrosion of metals and alloys.<sup>14,15</sup> Plant extract-based corrosion inhibitors are less expensive, biodegradable, and nontoxic than synthetic inhibitors and do not pose a risk to human health or the environment.<sup>16–27</sup> Therefore, eco-friendly corrosion inhibitors, also termed green alternatives, have been studied recently to replace poisonous and dangerous compounds. The culture contained a number of quinolizidine lupine family alkaloids, but multiflorine and lupanine were the most prevalent. In addition, sparteine, a dibasic quinolizidine alkaloid, is present in lupine extract.<sup>28–32</sup> The inhibitory effects of the lupine extract on Cu corrosion in 2 M H<sub>2</sub>NSO<sub>3</sub>H were investigated in this work using weight loss and electrochemical techniques. The acquired results were validated using an Fourier transform infrared (FT-IR) spectrometer, DFT computations, Fukui functions, Monte Carlo simulation, and an SEM microscope.

## 2. MATERIALS AND METHODS

**2.1. Preparation of the Plant Extract.** The lupine plant was cleaned, crushed, and dried to produce a fine powder. The plant samples were dried at 45 °C for the whole day. We extracted 50 g of fine powder with 250 mL of methanol using the Soxhlet apparatus for 12 h. To create a solid product that was crushed and freeze-dried, the filtrates from the earlier processes were concentrated.<sup>10,33</sup> In order to create the inhibitors, methanol was used to dilute a concentrated solution of lupine (1000 ppm). Our tests employed lupine extract at various doses ranging from 100 to 500 ppm. The chemical action of lupine extract was previously covered in Section 1. The main chemical components of lupine extract are shown in Figure 1.<sup>13,34</sup>

**2.2. Preparation of Copper Working Samples and Corrosive Media.** The samples used in this study were all made from copper. Before each test, the Cu samples had 200, 400, 600, 1200, and 2000 grit sandpaper surface polishing. For mass loss and electrochemical tests, the Cu specimens were chopped into rectangular forms with dimensions of 2.0, 2.0, 0.1 and 1.0, 1.0,

0.1 cm, respectively. Inhibitor solutions were generated in concentrations ranging from 100 to 500 ppm in 2 M aqueous H<sub>2</sub>NSO<sub>3</sub>H, with purified water and commercial sulfamic acid serving as the corrosive control medium.<sup>35</sup>

**2.3. Experimental Methods.** **2.3.1. Mass Loss Tests.** Gravimetric analysis is an often used corrosion method. This method is perfect for beginners because it is simple to use and does not require a lot of equipment. The sample is submerged in a corrosive solution at 25 °C for 3 h and has dimensions of 2 cm × 2 cm × 0.1 cm. The following equation was used to compute corrosion rates and corrosion inhibition effectiveness using various inhibitor concentrations<sup>36</sup>

$$C_R = \frac{K \times W}{At\rho} \quad (1)$$

where ( $C_R$ ) stands for corrosion rate, ( $W$ ) stands for mass loss, ( $t$ ) stands for immersion time, ( $\rho$ ) stands for copper density, and ( $K$ ) stands for corrosion constant, whose value is ( $8.76 \times 10^4$ ).

Inhibitor surface coverage ( $\theta$ ) and corrosion inhibition efficiency (IE) values were calculated using eqs 2 and 3, respectively.<sup>37</sup>

$$C_R = \frac{C_R^0 - C_R^i}{C_R^0} \times 100 \quad (2)$$

$$\theta = \frac{C_R^0 - C_R^i}{C_R^0} \quad (3)$$

where  $C_R^0$  and  $C_R^i$  reflect the corrosion rates with and without inhibitors, respectively.

**2.3.2. Electrochemical Tests.** In an electrochemical CS studio, a potentiodynamic polarization experiment was carried out. Three electrodes make up the three-electrode assembly: a reference electrode made of saturated calomel, a counter electrode made of platinum, and a working electrode made of copper with a 1 cm<sup>2</sup> surface exposed.<sup>38</sup> At 25 °C, all experiments were completed. Open-circuit potential (OCP) was established prior to each experiment by allowing the system to run for 30 min. Before each experiment, an open-circuit potential (OCP) is set up for 30 min. For this experiment, the power polarization potential range was from 1 to –250 mV with regard to OCP.<sup>39</sup> The EIS was then performed at OCP using a 5 mV AC signal with frequencies ranging from 100 kHz to 10 MHz.

**2.3.3. Theoretical Calculations.** Quantum chemical calculations employing generalized density functional theory (DFT) with the Becke three parameters Lee, Yang, and Parr (B3LYP) were carried out using Gaussian 09 software (Gaussian, Inc., CT, USA).<sup>40</sup> Many organic compounds' electrical characteristics and geometries can be precisely calculated using 6-311G++(d,p).

2.3.4. **Scanning Electron Microscopy (SEM).** The morphology of the copper surface was examined using a scanning electron microscope during the course of a 24 h immersion period in the presence or absence of a tested inhibitor.<sup>41</sup> Test was carried out with 500 ppm of the tested substance and 2 M H<sub>2</sub>NSO<sub>3</sub>H.

### 3. RESULTS

3.1. **Mass Loss (ML).** Figure 2 illustrates the results of a study of the influence of concentration on an inhibitor's ability to

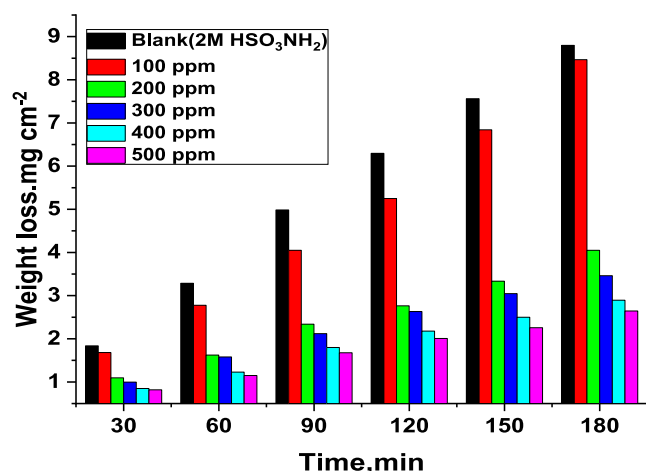


Figure 2. Copper mass loss at different lupine extract concentrations in 2 M H<sub>2</sub>NSO<sub>3</sub>H with and without immersion durations at 25 °C.

inhibit Cu in 2 M H<sub>2</sub>NSO<sub>3</sub>H. The Cu samples were placed in a 2 M H<sub>2</sub>NSO<sub>3</sub>H solution with varying amounts of lupine extract and corrosion inhibitors. For various concentrations of lupine extract in 2 M H<sub>2</sub>NSO<sub>3</sub>H, the corrosion rates and inhibitory effects calculated by using gravimetric methods are shown in Table 1. Table 1 shows that the essential lupine extract

Table 1. Several Measures of Inhibition for 2 M H<sub>2</sub>NSO<sub>3</sub>H's Corrosive Effects on Cu at Various Concentrations, Both with and without Lupine Extract

lupine extract concentration (ppm)	<i>k</i> , mg cm <sup>-2</sup> min <sup>-1</sup>	<i>θ</i>	<i>η</i> %
100	2.39	0.51	51.0
200	1.87	0.741	74.1
300	1.35	0.791	79.1
400	1.04	0.820	82.0
500	0.937	0.842	84.2

significantly inhibits Cu in 2 M H<sub>2</sub>NSO<sub>3</sub>H medium. The corrosion rate decreases as the inhibitor concentration rises, and the effectiveness of the inhibition also rises.<sup>42</sup> To maximize the effectiveness of inhibition, a protective coating must be formed via adsorption or by covering the electrode surface with inhibitor molecules.<sup>43</sup> This is interpreted as an increase in the efficiency with increasing concentration.

3.2. **Adsorption Isotherm.** Due to their efficiency in examining their adsorption mechanisms, two corrosion inhibitors have been examined through isothermal adsorption for a long time. The Temkin, Frumkin, Langmuir, and other common adsorption isotherms were compared, along with a number of others.<sup>44</sup> The results of the experiments were found to be consistent with Langmuir adsorption and might be applied

to improve our understanding of adsorption behavior. The following is a definition of Langmuir adsorption:<sup>45</sup>

$$\frac{C}{\theta} = \frac{1}{K_{\text{ads}}} + c \quad (4)$$

where *θ* stands for surface coverage, *K*<sub>ads</sub> means adsorption equilibrium constant, and *C* is the concentration of two corrosion inhibitors. The standard adsorption-free energy is calculated by the following formula<sup>46</sup>

$$K = \frac{1}{55.5} \exp\left(\frac{-\Delta G_{\text{ads}}}{RT}\right) \quad (5)$$

The values of *K*<sub>ads</sub> and  $-\Delta G_{\text{ads}}$  are listed in Figure 3. The lower the  $-\Delta G_{\text{ads}}$ , which generally correlates with greater *K*<sub>ads</sub>, the better the corrosion inhibitory characteristics.<sup>47</sup> The magnitude relation between the *K*<sub>ads</sub> values of multiflorine, sparteine, and lupanine is multiflorine > sparteine > lupanine; however, the relationship between  $-\Delta G_{\text{ads}}$  values is the opposite. The data show that multiflorine molecules strongly adsorb to Cu because of these events, which have a better corrosion inhibition effect than sparteine and lupanine. We are all aware that the type of adsorption of corrosion inhibitors depends on the value of  $-\Delta G_{\text{ads}}$ . When  $-\Delta G_{\text{ads}}$  falls below or equals 20 kJ/mol, physical adsorption takes place, and the adsorbent and sample are electrostatically drawn to one another.<sup>48</sup> As previously mentioned, chemical adsorption happens when  $-\Delta G_{\text{ads}} > 40$  kJ/mol, and during this process, the inhibitor molecule transferred electrons under friendly circumstances by sharing electrons with the Cu atoms on the surface.<sup>49</sup> In this investigation, chemical reactions demonstrated the inhibitor adsorption on Cu surfaces.

3.3. **Tests for Potentiodynamic Polarization.** Figure 4 depicts Cu's potentiodynamic polarization curves in a 2 M H<sub>2</sub>NSO<sub>3</sub>H solution, both with and without inhibitors. We examined the corrosion potential (*E*<sub>corr</sub>), corrosion current density (*i*<sub>corr</sub>), anodic and cathodic slopes (*β*<sub>a</sub>, *β*<sub>c</sub>), and corrosion inhibition efficacy (*η*%). Tafel extrapolation was used to calculate the corrosion current. Formulas were used to calculate *η*%.

$$\eta\% = \frac{i_{\text{corr}} - i_{\text{corr}}^0}{i_{\text{corr}}} \times 100 \quad (6)$$

The corrosion parameters acquired from the potentiodynamic polarization measurement are summarized in Figure 4. The inhibitive action of the inhibitor was examined using a potentiodynamic polarization analysis at various inhibitor doses. After the addition of additives to the sulfamic acid solution, the polarization curves in Figure 4 remain unchanged, indicating that the corrosion mechanism for Cu is unaffected.<sup>50</sup> Both anodic and cathodic curves have a mixed inhibitor character, which is a sign that corrosion current density is moving in the direction of lower value.<sup>51</sup> According to Table 2, different anodic and cathodic current densities were observed following the addition of a corrosion inhibitor, proving that lupine extract is a mixed-type corrosion inhibitor.<sup>52</sup> Lupine extract adsorption on Cu surfaces is indicated by the fact that *i*<sub>corr</sub> values decrease as inhibitor concentrations rise (Table 2). The difference between the inhibitor and inhibitor-free settings in terms of corrosion potential (*E*<sub>corr</sub>) is less than 85 mV, which suggests a combination of inhibitor-free circumstances.<sup>53</sup> A small change in *E*<sub>corr</sub> readings relative to the blank values can be used to demonstrate that both inhibitors have a mix-type

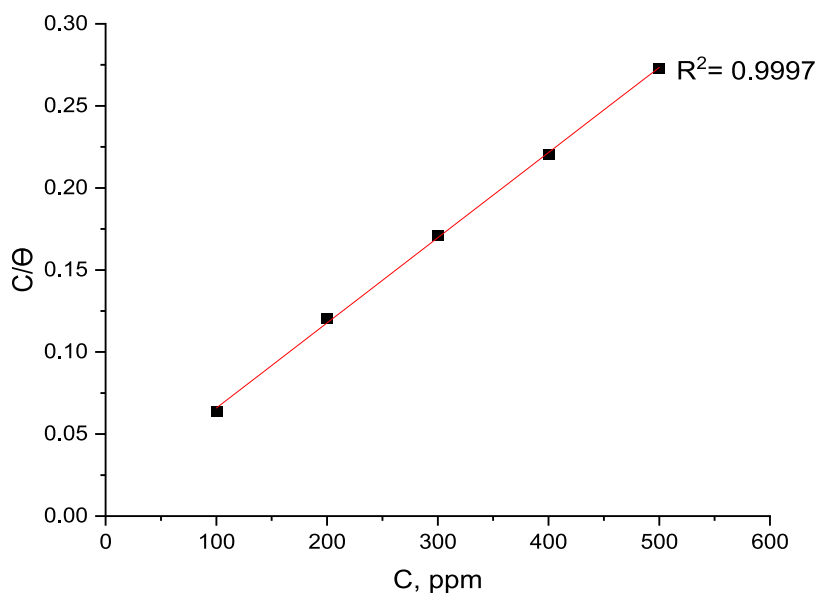


Figure 3. Cu adsorption graphs in 2 M  $\text{H}_2\text{NSO}_3\text{H}$  with and without various lupine extract consistencies at 25 °C.

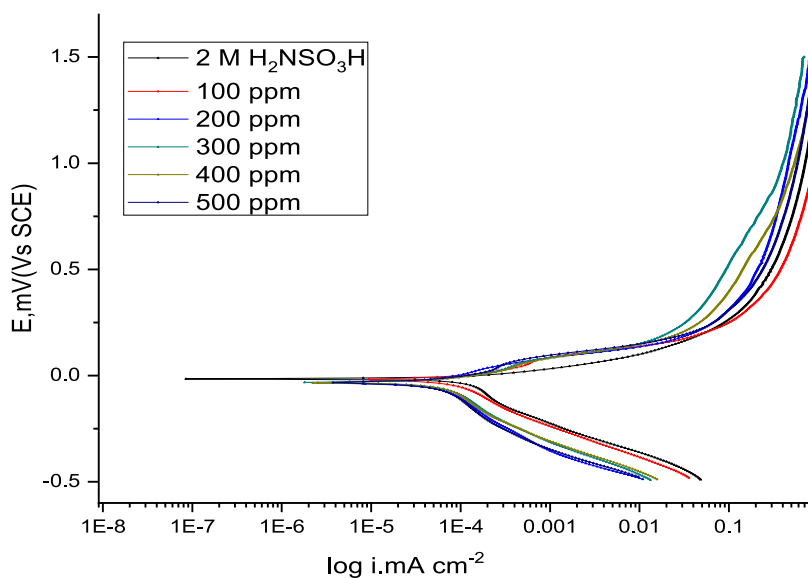


Figure 4. PP curves for Cu corrosion in 2 M  $\text{H}_2\text{NSO}_3\text{H}$  solution without and with varying dosages of lupine extract at 25 °C.

Table 2. Electrochemical Parameters Derived by the PP Method for the Corrosion of Cu in 2 M  $\text{H}_2\text{NSO}_3\text{H}$  in the Presence and Absence of Lupine Extract at 25 °C

Inh. (ppm)	$-E_{\text{corr}}$ (mV vs SCE)	$i_{\text{corr}}$ ( $\mu\text{A}/\text{cm}^2$ )	$\beta_c$ (mV/dec)	$\beta_a$ (mV/dec)	$k_{\text{corr}}$ (mm/y)	$\theta$	%IE
blank	589	301	248.6	66.1	148.3		
100	359	117	143.8	110.0	56.38	0.612	61.2
200	568	111	71.3	241.3	53.45	0.631	63.1
300	493	82.8	75.8	208.3	40.02	0.725	72.5
400	471	69.4	79.8	173	33.55	0.769	76.9
500	592.0	30.5	269.8	107.3	15.03	0.899	89.9

inhibitory effect that is primarily anodic in nature.<sup>54</sup> After the addition of lupine extract, an inhibitor was used to control the anode and cathode reactions. Lupine extract has a value of 89.9% at 500 ppm concentration. The stable development of the lupine extract adsorbed film on Cu surfaces can be attributed to this. This film lowers the current density at the anodic and cathodic

sites by shielding them from hydrogen evolution in 2 M  $\text{H}_2\text{NSO}_3\text{H}$  solution and metal dissolution at the anodic site.

### 3.4. Electrochemical Impedance Spectroscopy (EIS).

Electrochemical impedance spectroscopy (EIS) was used to analyze the behavior of the metal/solution contact in the absence and presence of inhibitors. Figure 5 illustrates an equivalent circuit, which is a parallel combination of the charge-

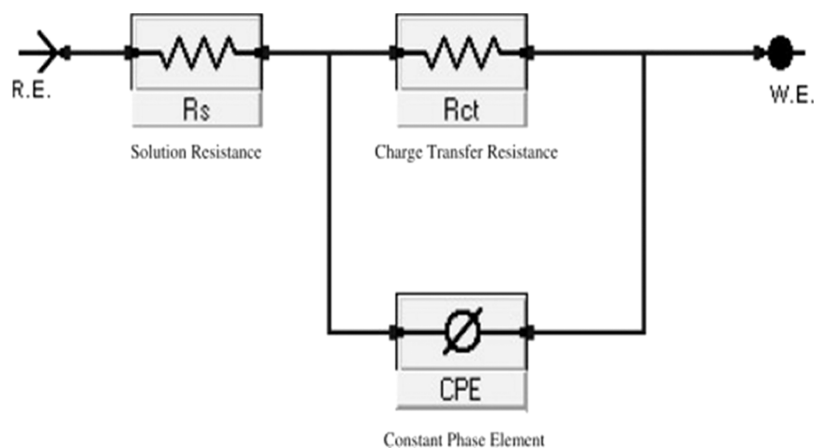


Figure 5. Equivalent circuit model used to fit the experimental results.

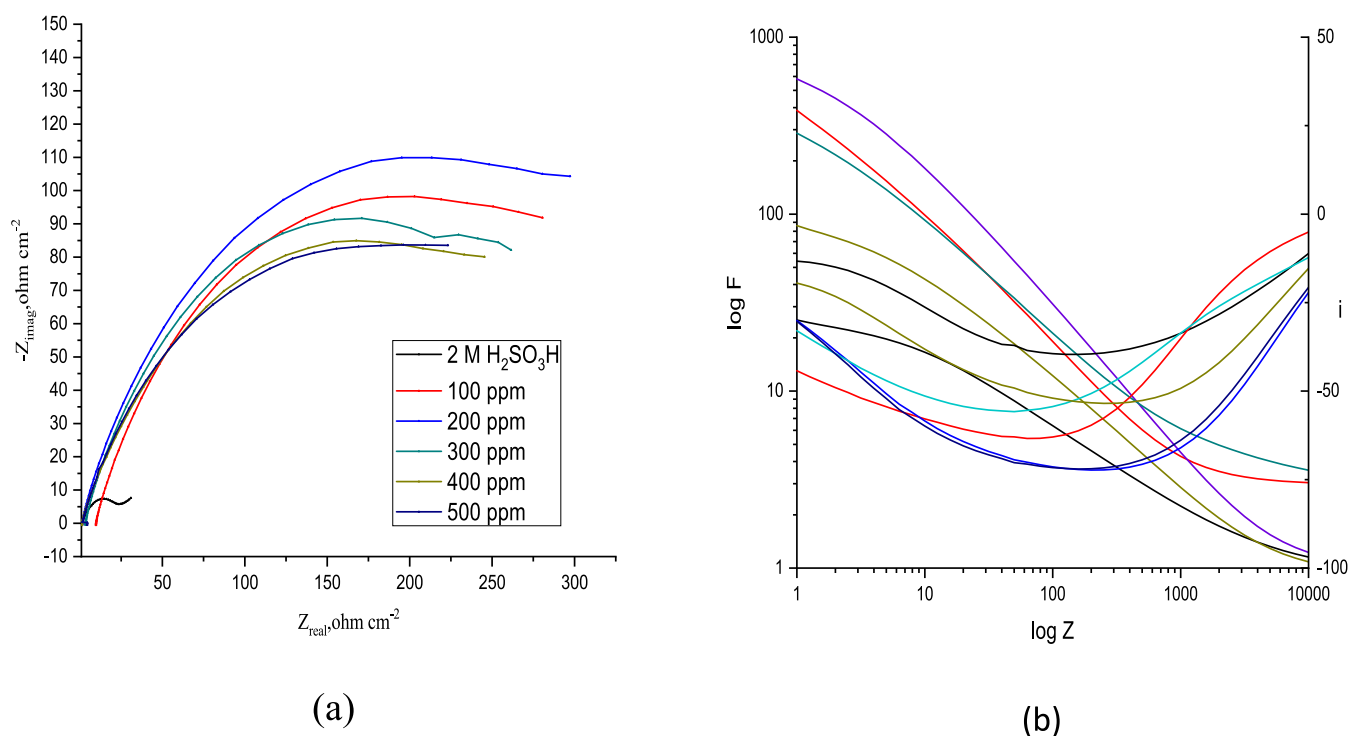


Figure 6. (a, b) Cu in 2 M  $\text{H}_2\text{NSO}_3\text{H}$  solutions with and without various dosages of lupine extract plotted using the (a) Nyquist and (b) Bode method at 25 °C.

Table 3. Electrochemical Parameters for the Corrosion of Cu 2 M  $\text{H}_2\text{NSO}_3\text{H}$  Solutions with and without the Presence of Various Dosages of Lupine Extract at 25 °C Determined by the EIS Approach

conc., ppm	$C_{dl}$ , $\mu\text{F cm}^{-2}$	$R_{ct}$ , $\Omega \text{ cm}^2$	$\alpha$	$Y_0 \times 10^{-4}$ , $\mu\Omega^{-1} \text{ sn m}^{-2}$	% IE	$X^2$
blank	11.2	19.74	0.69	7.2		0.0246
100	7.5	37.66	0.71	5.6	47.6	0.4391
200	4.87	51.69	0.69	6.3	61.8	0.0127
300	4.76	53.88	0.71	6.2	63.4	0.3990
400	4.18	60.44	0.69	6.3	67.3	0.4535
500	0.67	329.5	0.87	7.2	94.0	0.0046

transfer resistance ( $R_{ct}$ ) and the constant phase element (CPE), both in series with the solution resistance ( $R_s$ ) that is used to take into account all of the processes involved in the electrical response of the system. Figure 6a,b shows the Nyquist and Bode plots for Cu in an aggressive solution at 25 °C, both without and with various amounts of the lupine extract. Following 30 min of

immersion in a 2 M  $\text{H}_2\text{NSO}_3\text{H}$  solution, copper samples were examined for electrochemical characteristics using the lupine extract concentrations listed in Table 3. The Nyquist plots of lupine extract, which show that each capacitive loop reflects a single time constant, suggest that the kinetics of the electrochemical system is regulated by charge transfer. Indicating that

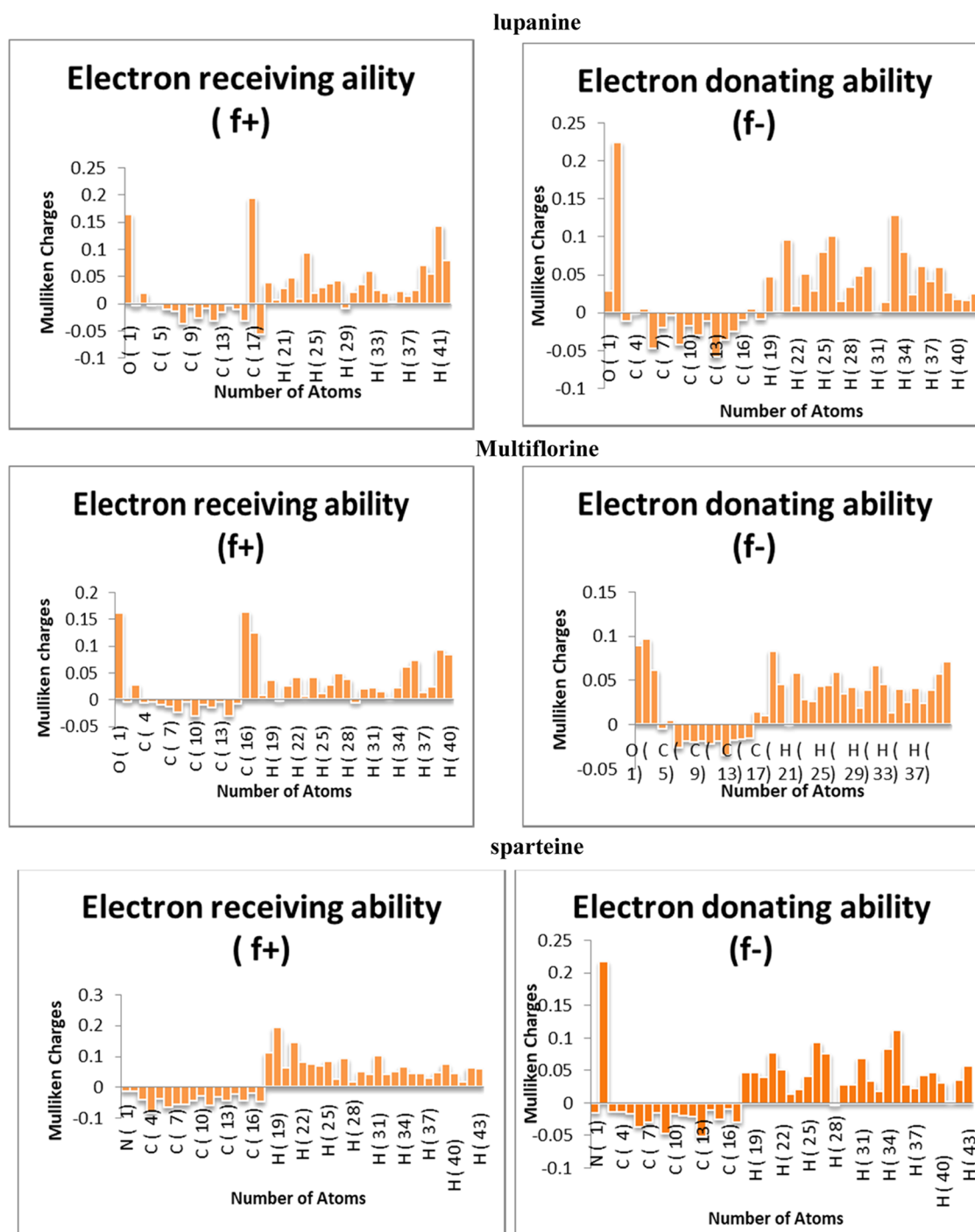


Figure 7. Diagram of Fukui function of the lupine extract inhibitor sparteine, multiflorine, and lupanine.

the addition of lupine extract to a 2 M  $\text{H}_2\text{NSO}_3\text{H}$  solution has no effect on the corrosion mechanism is Figure 6, which shows that the appearance of the curve is the same before and after the addition of inhibitors.<sup>55</sup> The rough surface of the Cu electrode causes an incomplete semicircle to appear in the Nyquist plots with a one-time constant. The addition of lupine extract to the 2 M  $\text{H}_2\text{NSO}_3\text{H}$  solution results in a noticeable increase in the capacitive loop diameter.<sup>56</sup> As the inhibitor's concentration rises, it either becomes adsorbed on the surface of Cu or thin films start to develop there. This protective layer significantly slows Cu corrosion in a 2 M  $\text{H}_2\text{NSO}_3\text{H}$  solution by reducing

Cu's active surface area and improving its corrosion resistance behavior.

$$C_{dl} = (Y_0 R_p^{1-n})^{1/n} \quad (7)$$

$$\eta\% = \frac{R_{P_{inh}} - R_{P_0}}{R_{P_{inh}}} \times 100 \quad (8)$$

Table 3 presents the EIS parameters. According to EIS data,  $C_{dl}$  values fall as lupine extract concentrations rise and  $R_p$  values rise. As a result, it is possible to draw the conclusion that molecules of lupine extract adsorbed on the Cu surface by displacing water

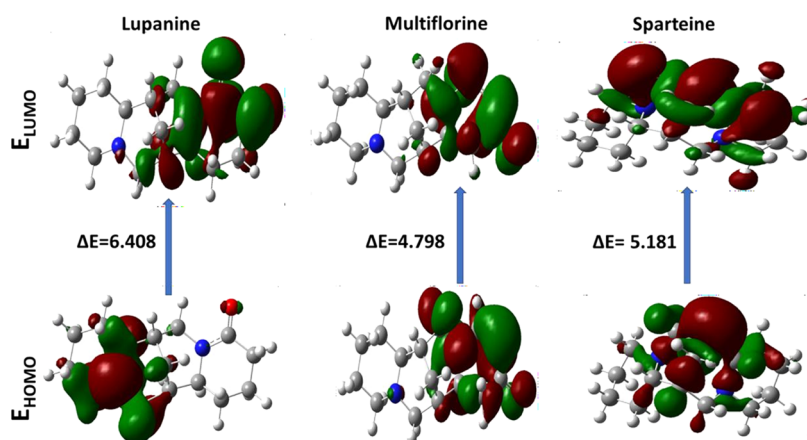


Figure 8. HOMO and LUMO molecular orbitals of sparteine, multiflorine, and lupanine.

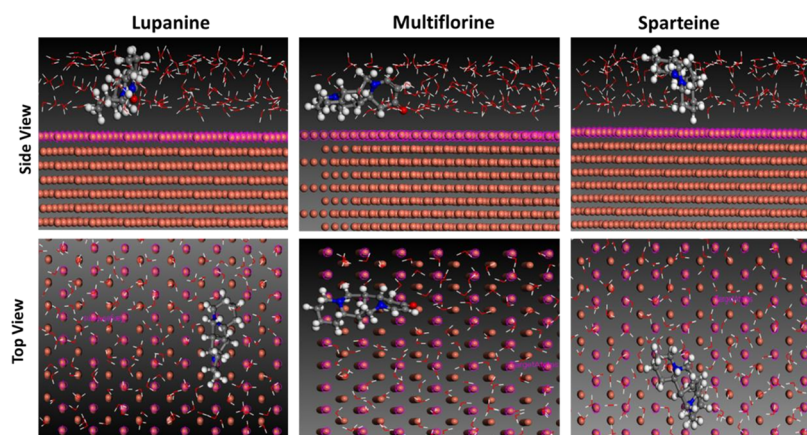


Figure 9. Adsorption of lupine extract compounds on the Cu surface.

Table 4. Lupine Extract Compound Adsorption Characteristics from Monte Carlo Simulation on the Cu(110) Surface

structure	total energy	adsorption energy	rigid adsorption energy	deformation energy	$E_{\text{ads}}$ , compound
Cu(110) – 1 lupanine	–2522.36	–2664.88	–2800.52	135.648	–16.771
Cu(110) – 1 multiflorine	–2571.21	–2649.14	–2779.51	130.364	–12.301
Cu(110) – 1 sparteine	–2550.89	–2669.88	–2802.54	132.650	–15.6295

molecules at the metal-to-water interface, resulting in slower rates of metal dissolution.<sup>57</sup> As a result, there is an increase in % values as the concentration of the lupine extract increases. At a 500 ppm concentration and 25 °C, the efficacy of the lupine extract as an inhibitor was determined to be 94%. This outcome is consistent with the inhibitor's adsorption on the Cu surface.

**3.5. Molecular Modeling.** **3.5.1. Fukui Function.** The most active locations of the optimized structures can be found by translating the electron density as a function of the number of electrons ( $N$ ) at a constant external potential using the Fukui function ( $f_x$ ).<sup>58</sup> Depending on the direction of electron transmission, the Fukui functions are determined using finite difference approximations based on population assessments of atoms in molecules and compounds.<sup>59</sup> At the atomic level,  $f^+$  denotes the capacity to accept electrons,  $f^-$  denotes the capacity to donate electrons, and  $f$  denotes the state of a free radical. While the multiflorine inhibitor has high electron density in atoms 11, 13, 14, and 30 due to CHO, NH, CN, C=O, and OCH<sub>3</sub>, respectively, it has low electron density in atoms 5, 7, and 20 due to conjugated carbons (Figure 7).

**3.5.2. HOMO–LUMO Molecule Orbital.** Figure 8 depicts the examined compound's lowest unoccupied molecular orbital (LUMO) and highest occupied molecular orbital (HOMO) density distributions in the aqueous phase. It shows that the color red has a high electron density and the color green has a low electron density.<sup>59</sup> The metal surface can contribute electrons when there is a high electron density. The metal surface in the green area receives electrons.<sup>60</sup> The distribution of these two areas must therefore be carefully taken into account because resonance is primarily caused by the links between the oxygen and nitrogen atoms on the benzene ring. The LUMO is centered on the carbon atoms in the meanwhile. Lower  $E$  values may indicate an improved inhibition efficiency. The  $E$  value can be used to assess the reactivity of the inhibitor molecule to the metal atom.<sup>61</sup> Due to its lower  $E$  value, multiflorous ( $E = 4.798$ ) is shown to be a better corrosion inhibitor than lupanine ( $E = 6.408$ ) and sparteine ( $E = 5.181$ ) as a result of the DFT calculations.

**3.5.3. MD Simulation.** The area where lupine extract was adsorbed onto the Cu(110) contact is shown in Figure 9. The parallel adsorption of multiflorine provides excellent protection

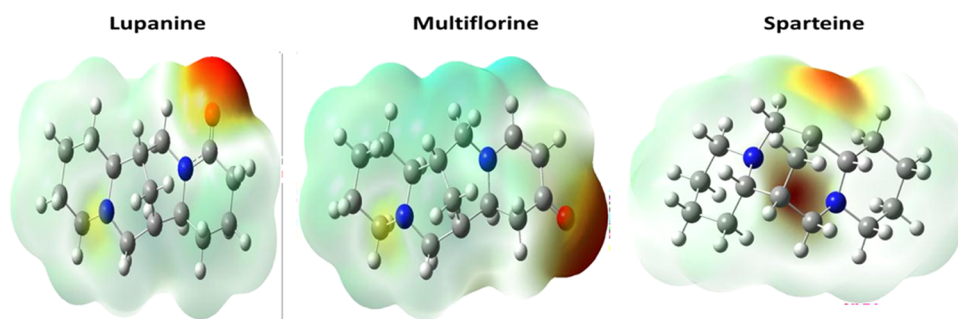


Figure 10. ESP pictures of the lupine extract.

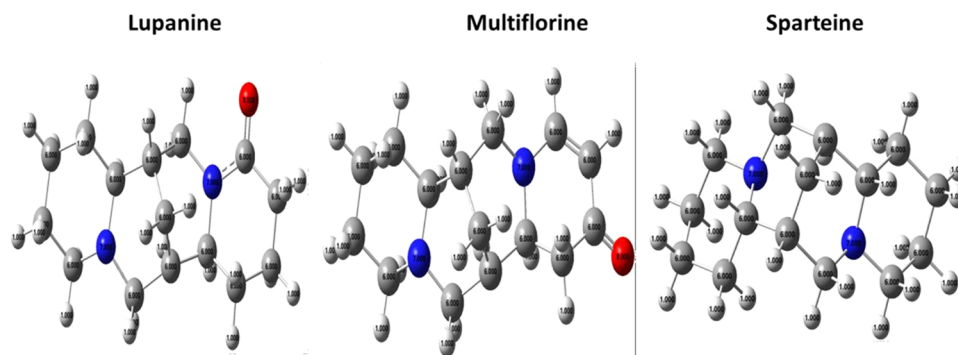


Figure 11. Mulliken atomic charges of compounds sparteine, multiflorine, and lupanine

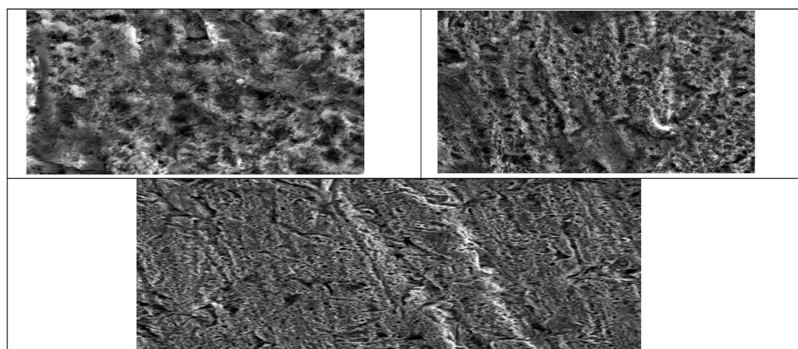


Figure 12. SEM images from Cu: (a) Cu alone, (b) after soaking time for 24 h in 2 M  $\text{H}_2\text{NSO}_3\text{H}$ , and (c) in the 500 ppm lupine extract inhibitor.

for the Cu substrate, but lupanine and sparteine require vertical adsorption. The greater adsorption energy of compound multiflorine suggests that it shelters the Cu surface more efficiently than compounds lupanine and sparteine.<sup>62</sup> Table 4 lists the results of the MD simulation for the energies of adsorption, stiff adsorption, and strain. Adsorption energy ( $E_{\text{ads}}$ ), which describes how firmly the inhibitor adheres to its substrate surface, has been computed. When molecules adsorb to metal surfaces, those that block adsorption release stiff adsorption power, and those that relax at metal surfaces release deformation power.<sup>63</sup> The Cu substrate was subjected to robust and spontaneous adsorption according to the lupine extract's negative  $E_{\text{ads}}$  values. Finally, inhibitors made from lupine extracts provide excellent corrosion defense (Figure 10).

**3.5.4. Electrostatic Potential (ESP) 2D Maps.** ESP maps make it possible to see how electrons are distributed and, consequently, where they are concentrated within each chemical.<sup>64</sup> The contour maps of electron density show that oxygen and nitrogen atoms appear to be advantageous interaction sites on the investigated molecule inhibitor, which

is consistent with the differences in functions between oxygen and the other atoms. A dark red outline surrounds the contact areas that produce the bonding connections between metal surfaces and inhibitor.<sup>65</sup> In the contour map of negative potential, lupine extract molecules in the aqueous phase are particularly encircled by a dark red color, whereas the green color is dispersed across the positive potential region at the DFT/B3LYP/6-31++G(2d,p) calculation level. The positive potential zone is colored green according to the contour electrostatic depiction.

**3.5.5. Charge Distribution.** High negative charge atoms or locations in the compound are more likely to donate electrons to the metal surfaces. Based on this information, oxygen and nitrogen atoms are the sites of the reactions within the molecules. Therefore, one of the most popular ways to present this characteristic is through Mulliken analysis.<sup>66</sup> Mulliken partial charges for the various atoms of the optimized molecules under study are illustrated in Figure 11. Mulliken charges can also show the locations of the inhibitor molecule binding on cell surfaces. On the basis of the charges of chelating atoms,

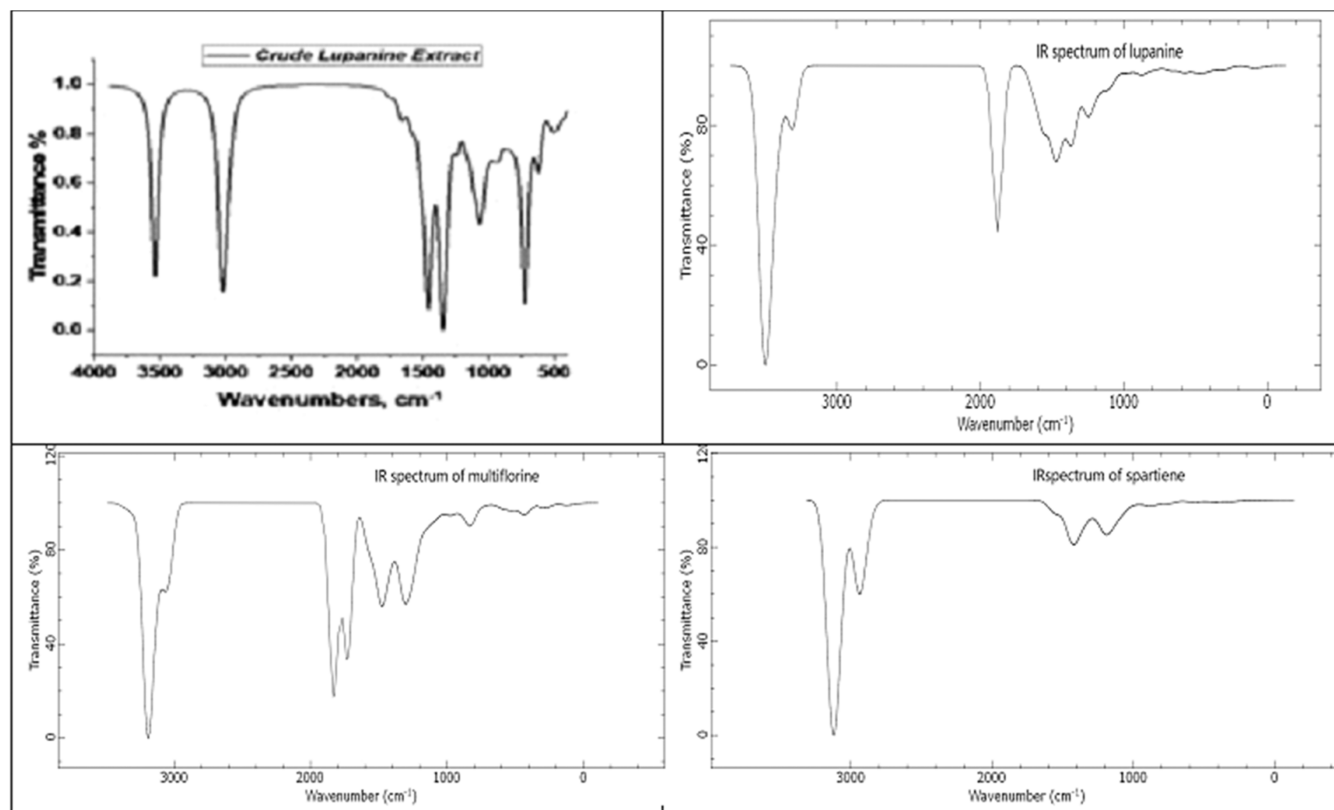


Figure 13. FTIR spectra of lupine extract.

inhibitors have been investigated to determine whether they stick to metallic surfaces. The likelihood that a metal's d orbital will get an electron donation rises as the negative Mulliken charge of an adsorption site decreases.<sup>67</sup> Mulliken charges for the lupine extract are broken down into carbon and heavy atoms (N and O). Therefore, in the anionic moiety of the compounds under study, charge-deficient metallic atoms should be drawn to suitable atoms.

**3.6. Scanning Electron Microscopy (SEM) Analysis.** The SEM image of Cu submerged in 2 M H<sub>2</sub>NSO<sub>3</sub>H for 24 h is shown in Figure 12 both with and without inhibitors for lupine extract. The roughness of the metal surface indicates Cu corrosion in sulfamic acid in the Cu surface SEM micrographs in Figure 12b without an inhibitor.<sup>68</sup> Figure 12c shows that the surface coverage increases in the presence of 500 ppm of inhibitors from lupine extract, which in turn causes the formation of the adsorbed compound on the metal surface. The surface is then covered by an inhibitor layer that successfully inhibits the dissolution of copper.

**3.7. FT-IR Analysis of the Extract and Corrosion Product.** The experimental IR spectrum of the lupine extract is shown in the image, together with the theoretical IR spectra of lupanine, multiflorine, and sparteine. Figure 13 shows the FTIR spectrum of a pure lupine extract. The –OH stretching frequency appears at 3419 cm<sup>-1</sup>,<sup>69</sup> the –CH stretching frequency at 2933 cm<sup>-1</sup>,<sup>70</sup> the C=O stretching frequency at 1654 cm<sup>-1</sup>,<sup>71</sup> the –C=C stretching frequency at (multiple bands) 1405–1547 cm<sup>-1</sup>,<sup>72</sup> the –CN stretching frequency at 1246 cm<sup>-1</sup>,<sup>73</sup> and the –CO stretching frequency at 1055 cm<sup>-1</sup>.<sup>74</sup> According to the theoretical infrared (IR) spectra of lupanine, multiflorine, and sparteine, the multiflorine IR is more like that of an experimental lupine extract than it is for lupanine and sparteine. This demonstrates that the primary ingredient in

lupine extract, multiflorine, is accountable for the inhibition process.

**3.8. Mechanism of Inhibition.** Any inhibitory mechanism's features are based only on the electron density at the reaction center. It is crucial to use polar groups that have selenium, phosphorus, sulfur, or nitrogen atoms as building blocks to create inhibitors.<sup>75</sup> The effectiveness of metal and inhibitor chemisorption is enhanced by increasing center electron density.<sup>76</sup> Due to lupine's chemical profile, the extract contains a large number of organic components. Cu surface oxidation is prevented by the components of the lupine extract adhering to it. These components' properties facilitate the adsorption process on the metal surface. The findings of the current study show how lupine extract can stop Cu corrosion in acid by adhering to the metal surface. The concentration of the inhibitor, the kind of metal, the temperature, and the quantity of adsorption sites are some of the variables that affect the inhibition process. Due to its chemical makeup, lupine extract exhibits a combination of chemisorption and physisorption. This information could be explained by the fact that organic molecules that have been adsorbed have the capacity to alter the behavior of the electrochemical corrosion processes in a variety of ways. Depending on how they interact, organic inhibitors can have a variety of different impacts on the metal substrate. Systems that use electrochemistry or surfaces may be affected by these interactions.

## 4. CONCLUSIONS

According to experimental tests, lupine extract derivatives work well as a mixed-type inhibitor to stop copper from corroding in a solution of 2 M H<sub>2</sub>NSO<sub>3</sub>H. Inhibition was evident when this substance formed Langmuir adsorption isotherms on the Cu

surfaces. Given that  $-\Delta G_{\text{ads}}$  had a negative value, it was assumed that the reaction was spontaneous. DFT revealed that the components in the structure of the lupine extract are able to transfer electrons from their highest occupied orbital (HOMO) to their lowest unoccupied orbital (LUMO). According to how well they can transfer electrons to metals and compounds, they do so. Ultimately, it was determined that the findings and measurements were in agreement.

## AUTHOR INFORMATION

### Corresponding Authors

Aya. M. Salem – Department of Basic Science, Higher Institute of Electronic Engineering (HIEE), Belbis 44621, Egypt;  
orcid.org/0000-0003-0675-5191; Email: ayasalem993@gmail.com

Merfat S. Al-Sharif – Department of Chemistry, College of Sciences, Taif University, Taif 21944, Saudi Arabia;  
Email: m.alshareef@tu.edu.sa

Complete contact information is available at:  
<https://pubs.acs.org/10.1021/acsomega.3c08211>

### Author Contributions

Conceptualization, methodology, project administration, and funding acquisition: M.S.A.-S.; software, validation, and formal analysis, writing, editing and data analysis, supervision: A.M.S. All authors have read and agreed to the published version of the manuscript.

### Funding

The researchers acknowledge the Deanship of Scientific Research, Taif University, for funding this work.

### Notes

The authors declare no competing financial interest.

## ACKNOWLEDGMENTS

The researchers acknowledge the Deanship of Scientific Research, Taif University, for funding this work.

## REFERENCES

- (1) Yassin, A.; Abdallah, Y. Characterization of PVVH/PEMA blend polymer with gold nanoparticles as corrosion inhibitors for N80 carbon steel in a 5% sulfamic acid solutions. *Delta Univ. Sci. J.* **2022**, *5* (2), 20–42, DOI: 10.21608/dusj.2022.275418.
- (2) Gu, T.; Tan, B.; Liu, J.; et al. Insight into the corrosion inhibition performance of Jasmine flower extract on copper in sulfuric acid medium using experimental and theoretical calculation methods. *J. Taiwan Inst. Chem. Eng.* **2023**, *150*, No. 105047.
- (3) Fonseca, I.; Picciochi, R.; Mendonça, M.; et al. The atmospheric corrosion of copper at two sites in Portugal: a comparative study. *Corros. Sci.* **2004**, *46* (3), 547–561.
- (4) Corvo, F.; Minotas, J.; Delgado, J.; et al. Changes in atmospheric corrosion rate caused by chloride ions depending on rain regime. *Corros. Sci.* **2005**, *47* (4), 883–892.
- (5) Sandberg, J.; Odnevall Wallinder, I.; Leygraf, C.; et al. Corrosion-induced copper runoff from naturally and pre-patinated copper in a marine environment. *Corros. Sci.* **2006**, *48* (12), 4316–4338.
- (6) Vera, R.; Delgado, D.; Rosales, B. M. Effect of atmospheric pollutants on the corrosion of high power electrical conductors—Part 2. Pure copper. *Corros. Sci.* **2007**, *49* (5), 2329–2350.
- (7) Vera, R.; Delgado, D.; Rosales, B. M. Effect of atmospheric pollutants on the corrosion of high power electrical conductors: Part 1. Aluminium and AA6201 alloy. *Corros. Sci.* **2006**, *48* (10), 2882–2900.
- (8) Abdel-Karim, A. M.; El-Shamy, A. M. A review on green corrosion inhibitors for protection of archeological metal artifacts. *J. Bio-Tribo-Corros.* **2022**, *8* (2), No. 35.
- (9) Thakur, A.; Kumar, A. Sustainable inhibitors for corrosion mitigation in aggressive corrosive media: a comprehensive study. *J. Bio-Tribo-Corros.* **2021**, *7*, 1–48.
- (10) Chukwuejim, S.; Utioh, A.; Choi, T. D.; et al. Lupin Seed Proteins: A Comprehensive Review of Composition, Extraction Technologies, Food Functionality, and Health Benefits. *Food Rev. Int.* **2023**, 1–24.
- (11) Domínguez, R.; Bermúdez, R.; Pateiro, M.; et al. Optimization and Characterization of Lupin Protein Isolate Obtained Using Alkaline Solubilization-Isoelectric Precipitation. *Foods* **2023**, *12* (20), 3875.
- (12) Ainouche, A. K.; Bayer, R. J. Phylogenetic relationships in *Lupinus* (Fabaceae: Papilionoideae) based on internal transcribed spacer sequences (ITS) of nuclear ribosomal DNA. *Am. J. Bot.* **1999**, *86* (4), 590–607.
- (13) Panasiewicz, K. Chemical Composition of Lupin (*Lupinus* spp.) as Influenced by variety and tillage system. *Agriculture* **2022**, *12* (2), 263.
- (14) Gao, X.; Wu, H. b.; Liu, M.; et al. Effect of annealing time on grain boundary characteristics of C71500 cupronickel alloy tubes with different deformation. *Mater. Charact.* **2020**, *169*, No. 110603.
- (15) Liu, M.; Li, J. In-situ Raman characterization of initial corrosion behavior of copper in neutral 3.5% (wt.) NaCl solution. *Materials* **2019**, *12* (13), 2164.
- (16) Alrefaee, S. H.; Rhee, K. Y.; Verma, C.; et al. Challenges and advantages of using plant extract as inhibitors in modern corrosion inhibition systems: Recent advancements. *J. Mol. Liq.* **2021**, *321*, No. 114666.
- (17) Barghout, N. A.; El Nemr, A.; Abd-El-Nabey, B. A.; et al. Use of orange peel extract as an inhibitor of stainless steel corrosion during acid washing in a multistage flash desalination plant. *J. Appl. Electrochem.* **2023**, *53* (2), 379–399.
- (18) Bilgiç, S. Plant extracts as corrosion inhibitors for aluminium in alkaline and in both acidic and alkaline environments—Review II. *Commun. - Fac. Sci., Univ. Ankara, Ser. B: Chem. Chem. Eng.* **2023**, *65* (1), 1–28.
- (19) Dehghani, A.; Ramezanzadeh, B. Rosemary extract inhibitive behavior against mild steel corrosion in tempered 1 M HCl media. *Ind. Crops Prod.* **2023**, *193*, No. 116183.
- (20) Fazal, B. R.; Becker, T.; Kinsella, B.; et al. A review of plant extracts as green corrosion inhibitors for CO2 corrosion of carbon steel. *npj Mater. Degrad.* **2022**, *6* (1), No. 5.
- (21) Hossain, N.; Islam, M. A.; Chowdhury, M. A. Advances of Plant-Extracted Inhibitors in Metal Corrosion Reduction—Future Prospects and Challenges. *Results Chem.* **2023**, *5*, No. 100883.
- (22) Huang, L.; Chen, W. Q.; Wang, S. S.; et al. Starch, cellulose and plant extracts as green inhibitors of metal corrosion: a review. *Environ. Chem. Lett.* **2022**, *20* (5), 3235–3264.
- (23) Kellal, R.; Left, D. B.; Azzi, M.; et al. Insight on the corrosion inhibition performance of *Glebionis coronaria* plant extract in various acidic mediums. *J. Appl. Electrochem.* **2023**, *53* (4), 811–832.
- (24) Salleh, S. Z.; Yusoff, A. H.; Zakaria, S. K.; et al. Plant extracts as green corrosion inhibitor for ferrous metal alloys: A review. *J. Cleaner Prod.* **2021**, *304*, No. 127030.
- (25) Tan, B.; Xiang, B.; Zhang, S.; et al. Papaya leaves extract as a novel eco-friendly corrosion inhibitor for Cu in H2SO4 medium. *J. Colloid Interface Sci.* **2021**, *582*, 918–931.
- (26) Verma, C.; Alfantazi, A.; Quraishi, M. A.; et al. Are extracts really green substitutes for traditional toxic corrosion inhibitors? Challenges beyond origin and availability. *Sustainable Chem. Pharm.* **2023**, *31*, No. 100943.
- (27) Wang, X.; Chen, L.; Yang, F.; et al. Corrosion inhibition mechanism and extraction technology of plant corrosion inhibitors: a review. *J. Adhes. Sci. Technol.* **2023**, *37*, 1–25.
- (28) Abd-El-Nabey, B.; El-Housseiny, S.; Abd-El-Fatah, M. Improved Pitting Corrosion Resistance of Stainless Steel 304 by Lupine extract in Hydrochloric Acid. *Int. J. Electrochem. Sci.* **2022**, *17* (10), No. 22101, DOI: 10.20964/2022.10.34.

- (29) Abdel-Shafi, S.; El-Nemr, M.; Enan, G.; et al. Isolation and Characterization of Antibacterial Conglutinins from Lupine Seeds. *Molecules* **2023**, *28* (1), 35.
- (30) Eldin, S. M. S.; Shawky, E.; Ghareeb, D. A.; et al. Metabolomics and chemometrics depict the changes in the chemical profile of white lupine (*Lupinus albus* L.) bioactive metabolites during seed germination. *Food Chem.* **2023**, *418*, No. 135967.
- (31) Struti, D. I.; Mierlita, D.; Simeanu, D.; et al. The effect of dehulling lupine seeds (*Lupinus albus* L.) from low-alkaloid varieties on the chemical composition and fatty acids content. *Rev. Chim.* **2020**, *71* (4), 59–70, DOI: 10.37358/RC.20.4.8043.
- (32) Zalewski, K.; Nitkiewicz, B.; Stolarski, M.; et al. The influence of exogenous methyl jasmonate on the germination and, content and composition of flavonoids in extracts from seedlings of yellow and narrow-leaved lupine. *J. Food Compos. Anal.* **2020**, *87*, No. 103398.
- (33) Khater, M.; et al. Changes in some physiological and biochemical parameters of lupine plant via two bio-stimulant yeast extract and folic acid. *J. Mater. Environ. Sci.* **2023**, *14* (3), 373–383.
- (34) Pereira, A.; Ramos, F.; Sanches Silva, A. Lupin (*Lupinus albus* L.) seeds: Balancing the good and the bad and addressing future challenges. *Molecules* **2022**, *27* (23), 8557.
- (35) Zhang, L.; Pan, Y.; Xu, K.; et al. Corrosion behavior of concrete fabricated with lithium slag as corrosion inhibitor under simulated acid rain corrosion action. *J. Cleaner Prod.* **2022**, *377*, No. 134300.
- (36) Abdullah, H.; Anae, R.; Khadom, A. Expired Methem drug as a corrosion inhibitor for aluminum in 1 M HCl solution: Experimental and theoretical studies. *Int. J. Corros. Scale Inhib.* **2022**, *11*, 1355–1373.
- (37) Mohamed, A.; Visco, D., Jr; Bastidas, D. Effect of cations on the activity coefficient of NO<sub>2</sub>–/NO<sub>3</sub>–corrosion inhibitors in simulated concrete pore solution: An electrochemical thermodynamics study. *Corros. Sci.* **2022**, *206*, No. 110476.
- (38) Ma, I. A. W.; Ammar, S.; Kumar, S. S. A.; et al. A concise review on corrosion inhibitors: types, mechanisms and electrochemical evaluation studies. *J. Coat. Technol. Res.* **2022**, *19*, 241–268.
- (39) Khamaysa, O. M. A.; Selatnia, I.; Lgaz, H.; et al. Hydrazone-based green corrosion inhibitors for API grade carbon steel in HCl: Insights from electrochemical, XPS, and computational studies. *Colloids Surf., A* **2021**, *626*, No. 127047.
- (40) Eno, E. A.; Mbonu, J. I.; Louis, H.; et al. Antimicrobial activities of 1-phenyl-3-methyl-4-trichloroacetyl-pyrazolone: Experimental, DFT studies, and molecular docking investigation. *J. Indian Chem. Soc.* **2022**, *99* (7), No. 100524.
- (41) Benzbiria, N.; Thoume, A.; Echihi, S.; et al. Coupling of experimental and theoretical studies to apprehend the action of benzodiazepine derivative as a corrosion inhibitor of carbon steel in 1M HCl. *J. Mol. Struct.* **2023**, *1281*, No. 135139.
- (42) Vuong, B. X.; Huynh, T. L.; Tran, T. Q. N.; et al. Corrosion inhibition of carbon steel in hydrochloric acid solution by self-formation of a *Malpighia glabra* leaf extract-based organic film. *Mater. Today Commun.* **2022**, *31*, No. 103641.
- (43) Al-Amiery, A. A.; Al-Azzawi, W. K.; Isahak, W. N. R. W. Isatin Schiff base is an effective corrosion inhibitor for mild steel in hydrochloric acid solution: Gravimetric, electrochemical, and computational investigation. *Sci. Rep.* **2022**, *12* (1), No. 17773.
- (44) Wei, H.; Heidarshenas, B.; Zhou, L.; et al. Green inhibitors for steel corrosion in acidic environment: state of art. *Mater. Today Sustainability* **2020**, *10*, No. 100044.
- (45) Kokalj, A. On the use of the Langmuir and other adsorption isotherms in corrosion inhibition. *Corros. Sci.* **2023**, *217*, No. 111112.
- (46) Li, H.; Zhang, S.; Tan, B.; et al. Investigation of Losartan Potassium as an eco-friendly corrosion inhibitor for copper in 0.5 M H<sub>2</sub>SO<sub>4</sub>. *J. Mol. Liq.* **2020**, *305*, No. 112789.
- (47) Chaudhary, S.; Tak, R. K. Natural corrosion inhibition and adsorption characteristics of *tribulus terrestris* plant extract on aluminium in hydrochloric acid environment. *Biointerface Res. Appl. Chem.* **2022**, *12* (2), 2603–2617.
- (48) Yan, T.; Zhang, S.; Feng, L.; et al. Investigation of imidazole derivatives as corrosion inhibitors of copper in sulfuric acid: combination of experimental and theoretical researches. *J. Taiwan Inst. Chem. Eng.* **2020**, *106*, 118–129.
- (49) Li, W.; Tan, B.; Zhang, S.; et al. Insights into triazole derivatives as potential corrosion inhibitors in CMP process: Experimental evaluation and theoretical analysis. *Appl. Surf. Sci.* **2022**, *602*, No. 154165.
- (50) Saraswat, V.; Yadav, M. Improved corrosion resistant performance of mild steel under acid environment by novel carbon dots as green corrosion inhibitor. *Colloids Surf., A* **2021**, *627*, No. 127172.
- (51) Zhang, W.; Zhang, D.; Li, X.; et al. Excellent performance of dodecyl dimethyl betaine and calcium gluconate as hybrid corrosion inhibitors for Al alloy in alkaline solution. *Corros. Sci.* **2022**, *207*, No. 110556.
- (52) Kahkesh, H.; Zargar, B. Corrosion protection evaluation of *Allium Jesdianum* as a novel and green source inhibitor for mild steel in 1M HCl solution. *J. Mol. Liq.* **2021**, *344*, No. 117768.
- (53) Toghan, A.; Fawzy, A.; Alakhras, A. I.; et al. Electrochemical and theoretical examination of some imine compounds as corrosion inhibitors for carbon steel in oil wells formation water. *Int. J. Electrochem. Sci.* **2022**, *17* (12), No. 2212108.
- (54) Weeraratne, A. D. K. I. Induction And Prevention Of Electron Transport In Langmuir-Blodgett Films Of 3d-Based Metallosurfactants: Studies On Current Rectification And Corrosion Inhibition. Dissertation, Wayne State University, 2021.
- (55) Al-nami, S. Y.; Alturki, A. M.; Wahba, A. M. Eco-Friendly Methanolic Myrrh Extract Corrosion Inhibitor for Aluminum in 1 M HCl. *ACS Omega* **2023**, *8*, 30917–30928, DOI: 10.1021/acsomega.3c02009.
- (56) Fouda, A.; Wahba, A.; Eissa, M. Aluminum corrosion prevention in 1.0 M HCl solution by *Cytosiera myrica* extract: An experimental and biological study. *J. Indian Chem. Soc.* **2022**, *99* (8), No. 100619.
- (57) Salem, A.; Wahba, A.; Hossiany, A. E.; et al. Experimental and computational chemical studies on the corrosion inhibitive properties of metamizole sodium pharmaceutical drug compound for CS in hydrochloric acid solutions. *J. Indian Chem. Soc.* **2022**, *99* (12), No. 100778.
- (58) Atlam, F. M.; Mohamed, A. A.; Awad, M. K. New Theoretical Insights about Anticorrosive Effects and Adsorption Mechanism of Some  $\alpha$ -Amino Acids on Al Surface: DFT, MEP, FMO, NBO, QSAR, Fukui Functions and Monte Carlo Simulation. *Prot. Met. Phys. Chem. Surf.* **2022**, *58* (5), 1054–1070.
- (59) Khadom, A. A.; Kadhim, M. M.; Anae, R. A.; et al. Theoretical evaluation of *Citrus Aurantium* leaf extract as green inhibitor for chemical and biological corrosion of mild steel in acidic solution: Statistical, molecular dynamics, docking, and quantum mechanics study. *J. Mol. Liq.* **2021**, *343*, No. 116978.
- (60) Abdelaziz, S.; Benamira, M.; Messaadia, L.; et al. Green corrosion inhibition of mild steel in HCl medium using leaves extract of *Arbutus unedo* L. plant: An experimental and computational approach. *Colloids Surf., A* **2021**, *619*, No. 126496.
- (61) Dehghani, A.; Bahlakeh, G.; Ramezanzadeh, B. A detailed electrochemical/theoretical exploration of the aqueous Chinese gooseberry fruit shell extract as a green and cheap corrosion inhibitor for mild steel in acidic solution. *J. Mol. Liq.* **2019**, *282*, 366–384.
- (62) Boulhaoua, M.; El Hafi, M.; Zehra, S.; et al. Synthesis, structural analysis and corrosion inhibition application of a new indazole derivative on mild steel surface in acidic media complemented with DFT and MD studies. *Colloids Surf., A* **2021**, *617*, No. 126373.
- (63) Verma, D. K.; Aslam, R.; Aslam, J.; et al. Computational modeling: theoretical predictive tools for designing of potential organic corrosion inhibitors. *J. Mol. Struct.* **2021**, *1236*, No. 130294.
- (64) Shaban, M. M.; El Basiony, N. M.; Radwan, A. B.; et al. Electrochemical Investigation of C-Steel Corrosion Inhibition, In Silico, and Sulfate-Reducing Bacteria Investigations Using Pyrazole Derivatives. *ACS Omega* **2023**, *8*, 30068–30080, DOI: 10.1021/acsomega.3c02333.
- (65) Al-Moubaraki, A. H.; Chaouiki, A.; Alahmari, J. M.; et al. Development of natural plant extracts as sustainable inhibitors for

efficient protection of mild steel: Experimental and first-principles multi-level computational methods. *Materials* **2022**, *15* (23), 8688.

(66) Mohamed, A.; Martin, U.; Bastidas, D. M. Adsorption and surface analysis of sodium phosphate corrosion inhibitor on carbon steel in simulated concrete pore solution. *Materials* **2022**, *15* (21), 7429.

(67) Abu-Rayyan, A.; Al Jahdaly, B. A.; AlSalem, H. S.; et al. A study of the synthesis and characterization of new acrylamide derivatives for use as corrosion inhibitors in nitric acid solutions of copper. *Nanomaterials* **2022**, *12* (20), 3685.

(68) Tan, B.; Zhang, S.; Qiang, Y.; et al. Experimental and theoretical studies on the inhibition properties of three diphenyl disulfide derivatives on copper corrosion in acid medium. *J. Mol. Liq.* **2020**, *298*, No. 111975.

(69) Prabhu, R.; Roopashree, B.; Jeevananda, T.; et al. Synthesis and corrosion resistance properties of novel conjugated polymer-Cu<sub>2</sub>Cl<sub>4</sub>L<sub>3</sub> composites. *Mater. Sci. Energy Technol.* **2021**, *4*, 92–99.

(70) Bernath, P. F.; Sibert, E. L., III Cyclohexane vibrations: High-resolution spectra and anharmonic local mode calculations. *J. Phys. Chem. A* **2020**, *124* (48), 9991–10000.

(71) Alhazmi, H. A. FT-IR spectroscopy for the identification of binding sites and measurements of the binding interactions of important metal ions with bovine serum albumin. *Sci. Pharm.* **2019**, *87* (1), 5.

(72) Oliveros, A. N.; Pimentel, J. A. I.; de Luna, M. D. G.; et al. Visible-light photocatalytic diclofenac removal by tunable vanadium pentoxide/boron-doped graphitic carbon nitride composite. *Chem. Eng. J.* **2021**, *403*, No. 126213.

(73) Suzuki, K.; Katayama, K.; Sumii, Y.; et al. Vibrational analysis of acetylcholine binding to the M<sub>2</sub> receptor. *RSC Adv.* **2021**, *11* (21), 12559–12567.

(74) Yerezhep, D.; Akylbayeva, A.; Golikov, O.; et al. Analysis of Vibrational Spectra of Tetrafluoroethane Glasses Deposited by Physical Vapor Deposition. *ACS Omega* **2023**, *8*, 19567–19574, DOI: 10.1021/acsomega.3c00985.

(75) Abd El-Lateef, H. M.; Shaaban, S.; Khalaf, M. M.; et al. Synthesis, experimental, and computational studies of water soluble anthranilic organoselenium compounds as safe corrosion inhibitors for J55 pipeline steel in acidic oilfield formation water. *Colloids Surf., A* **2021**, *625*, No. 126894.

(76) Bahlakeh, G.; Dehghani, A.; Ramezanzadeh, B.; et al. Highly effective mild steel corrosion inhibition in 1 M HCl solution by novel green aqueous Mustard seed extract: Experimental, electronic-scale DFT and atomic-scale MC/MD explorations. *J. Mol. Liq.* **2019**, *293*, No. 111559.